Deterministic Loading of Microwaves onto an Artificial Atom Using a Time-Reversed Waveform

Citation for the original published paper (version of record):
Lin, W., Lu, Y., Wen, P. et al (2022). Deterministic Loading of Microwaves onto an Artificial Atom Using a Time-Reversed Waveform. Nano Letters, 22(20): 8137-8142.
http://dx.doi.org/10.1021/acs.nanolett.2c02578

(article starts on next page)

NANO LETTERS

pubs.acs.org/NanoLett
Letter

Deterministic Loading of Microwaves onto an Artificial Atom Using a Time-Reversed Waveform

Wei-Ju Lin, Yong Lu,*, Ping Yi Wen, Yu-Ting Cheng, Ching-Ping Lee, Kuan Ting Lin, Kuan Hsun Chiang, Ming Che Hsieh, Ching-Yeh Chen, Chin-Hsun Chien, Jia Jhan Lin, Jeng-Chung Chen, Yen Hsiang Lin, Chih-Sung Chuu, Franco Nori, Anton Frisk Kockum, Guin Dar Lin, Per Delsing, and Io-Chun Hoi*

Cite This: *Nano Lett.* 2022, 22, 8137−8142

ABSTRACT: Loading quantum information deterministically onto a quantum node is an important step toward a quantum network. Here, we demonstrate that coherent-state microwave photons with an optimal temporal waveform can be efficiently loaded onto a single superconducting artificial atom in a semi-infinite one-dimensional (1D) transmission-line waveguide. Using a weak coherent state (the number of photons (N) contained in the pulse $\ll 1$) with an exponentially rising waveform, whose time constant matches the decoherence time of the artificial atom, we demonstrate a loading efficiency of 94.2% ± 0.7% from 1D semifree space to the artificial atom. The high loading efficiency is due to time-reversal symmetry: the overlap between the incoming wave and the time-reversed emitted wave is up to 97.1% ± 0.4%. Our results open up promising applications in realizing quantum networks based on waveguide quantum electrodynamics.

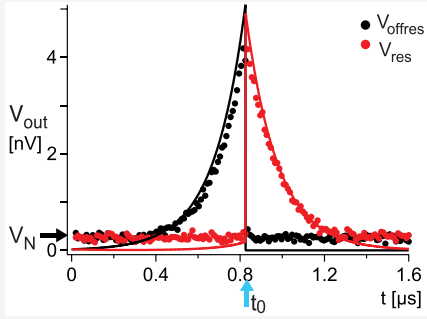

KEYWORDS: *Quantum network, photon loading, waveguide quantum electrodynamics, superconducting artificial atom*

Quantum networks,[1] consisting of quantum nodes and quantum channels, are a topic of intense research, spurred by the vision of a global quantum Internet.[2] Quantum nodes can process quantum information, whereas quantum channels can transmit it. The connectivity and scalability of quantum networks strongly depend on the ability to deterministically load quantum information from photons in quantum channels (e.g., free space) onto quantum nodes (e.g., qubits). This loading requires a strong interaction between the qubit and the photons, but this is very hard to achieve in three-dimensional (3D) free space due to a spatial mode mismatch.[3] Attempts have been made using atomic ensembles[4] to enhance the atom−field interaction. However, the loading efficiency only reached 20%.

A strong interaction between a single artificial atom (a superconducting qubit) and propagating microwave photons has been achieved in a one-dimensional (1D) open transmission line.[5−8] This has enabled many important quantum−optical experiments in 1D waveguide quantum electrodynamics (QED) in superconducting circuits in the past decade.[5−7,9−23] Temporal dynamics has been studied for both a single artificial atom in such a system[24] and a single real atom in free space.[25−27] Moreover, single-photon emission from superconducting qubits has also been implemented,[28−32] where the qubit absorbs only one photon from many input photons of the excitation pulse, leading to a very low loading efficiency. Impressive progress has been achieved when using a cavity for loading[33] (catching) in the optical (microwave[34,35]) regime and for quantum-state transfer.[36] Recently, deterministic qubit entanglement in a quantum network has been demonstrated through the standing-wave modes in a multimode cavity (a long cable) between two nodes.[37] In this type of setup, the distance between nodes will be limited and precise timing is required. However, deterministic loading of propagating photons directly onto a single atom (qubit) in the time domain, which would be an important component in a quantum network, has not yet been achieved. Such an interface would be preferable to enable quantum computation at the node without needing to convert the loaded quantum state further. Moreover, as compared to the methods in refs 33−37, our system is more compact and scalable, since no cavity is needed. Additionally, the resonance frequency of a superconducting qubit can be made tunable over a wide range[13,38] to allow the loading of photons at different wavelengths.

In this Letter, we demonstrate that photons in a weak coherent state can be efficiently loaded onto a single artificial

Received: June 30, 2022
Revised: September 28, 2022
Published: October 6, 2022

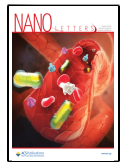

https://doi.org/10.1021/acs.nanolett.2c02578
Nano Lett. 2022, 22, 8137−8142

atom in a semi-infinite 1D free space. Our sample, depicted in Figure 1, is a superconducting circuit with a transmon qubit[38]

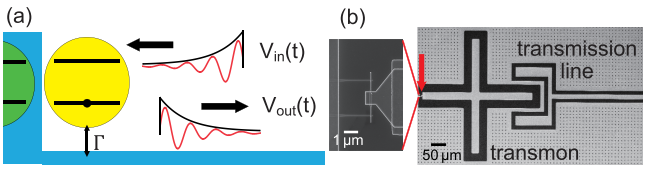

Figure 1. (a) Setup sketch. A superconducting artificial atom (yellow) in a semi-infinite 1D space, terminated by a mirror. The green half-disk is the mirror image of the yellow atom, indicating that propagating microwaves can interact with the atom twice, instead of once in the open transmission line case. Here, the mirror is used to ensure that the loaded photons can only emit into a single waveguide channel and enhance the maximal loading efficiency compared to the case of a qubit along an infinite transmission line. A resonant coherent drive with voltage $V_{in}(t)$ and exponentially rising waveform is sent toward the atom. After interaction with strength Γ between the atom and the input field, the atom emits an exponentially decaying output field $V_{out}(t)$. (b) Photo of sample 2 showing a transmon qubit located at the end of a transmission line, terminated by an open-end capacitor, which can be seen as having a mirror at a distance equal to 0. The transmon contains a superconducting quantum interference device (SQUID, indicated by the red arrow and magnification shown on the left) loop. Therefore, the atomic resonance frequency is tunable by an external magnetic flux.

coupled to a 1D semi-infinite waveguide, terminated by a mirror.[13,39] We perform experiments using a weak coherent state with exponentially rising (the time-reversed shape of a photon emitted by decay) waveforms. When an incident exponentially rising coherent state interacts with the qubit, destructive interference between the atomic emission and the incident field reflecting from the mirror leads to extinction of the output field. This perfect destructive interference occurs when mode matching is achieved. After the pulse is turned off, the atom emits an exponentially decaying field. The loading efficiency is characterized by the ratio of the coherent output energy and the coherent input energy, and the symmetry factor is characterized by the overlap between the incoming wave and the time-reversed emitted wave. In a perfect loading process with excitation and emission in the same line and a fixed coupling, the incoming wave and the emitted wave are time-reversed versions of each other. We achieved a loading efficiency and symmetry factor up to 94.2% ± 0.7% and 97.1% ± 0.4%, respectively.

We have measured two samples in this work. We first characterize the transmon qubit using single- and two-tone spectroscopy[40,41] where we obtain the qubit transition frequency (ω_{10}) and the relaxation rate (Γ), and $\gamma = 1/T_2$ with T_2 being the decoherence time. The extracted parameters are summarized in Table 1. For both samples, the values of $\gamma/2\pi$ are around 1 MHz.

We can also easily study the qubit dynamics in the time domain by using a digitizer with nanosecond resolution where our qubit dynamics is on the order of $T_2 \sim 150$ ns. Although the value of Γ is weak compared to many other experiments in superconducting waveguide QED,[5,16,17] the qubit-field coupling is still in the strong coupling regime, where Γ is much greater than $\Gamma_{\phi,n} = \Gamma_n/2 + \Gamma_\phi$ with Γ_ϕ being the pure dephasing rate and Γ_n being the nonradiative relaxation rate. We use all these extracted parameters to simulate the qubit response in the time-domain measurements in the rest of the paper. Further details on the experimental setup and characterization of the two samples are given in Sections S1 and S2 in the Supporting Information.

We now study the time dynamics of the qubit[42] response to a short pulse. We input an exponentially rising pulse with voltage amplitude

$$V_{in}(t) = V\Theta(t_0 - t)e^{(t-t_0)/\tau} \tag{1}$$

where Θ is the Heaviside step function, t_0 is the time when the pulse is turned off, and τ is the characteristic time of the exponentially rising waveform. Given V and τ, the number of photons (N) contained in the pulse $\left[N = \int_0^{t_0} P_{in}(t)\,dt/(\hbar\omega_{10})\right]$ is fixed; $P_{in}(t) = V_{in}(t)^2/(2Z_0)$ where $P_{in}(t)$ is the input power and Z_0 is the 50 Ω impedance of the transmission line. For example, $N = 0.09$ for $V^2/(2Z_0) = -144$ dBm (the critical power in the single-tone spectroscopy) and $\tau = 145$ ns (close to T_2). For further comparison, we also study three other input pulse shapes in Section S4 in the Supporting Information: exponentially decaying, square, and Gaussian.

We fix $N = 0.09$ and vary the characteristic time (τ) from 40 to 600 ns (see Figure S3 in the Supporting Information). For resonant excitation, input−output theory gives[43]

$$\alpha_{out}(t) = \alpha_{in}(t) + \sqrt{\Gamma}\langle\hat{\sigma}_-(t)\rangle \tag{2}$$

where α_{out} (α_{in}) is the amplitude of the output (input) coherent field in units of $\sqrt{\text{photons/s}}$ and $\hat{\sigma}_\pm$ is the atomic raising/lowering operator. This gives the Rabi frequency $\Omega(t) = 2\sqrt{\Gamma}\alpha_{in}(t) = k\sqrt{P_{in}(t)}$. The atom-field coupling constant (k) is calibrated by frequency-domain characterization (see Figure S2 in the Supporting Information), which allows one to calculate V_{out} at the sample.

The dynamics of the output field is governed by $\langle\hat{\sigma}_-(t)\rangle$, which is given by the Bloch equations

$$\partial_t\langle\hat{\sigma}_\pm\rangle = -\gamma\langle\hat{\sigma}_\pm\rangle + \Omega(t)\langle\hat{\sigma}_z\rangle/2 \tag{3}$$

$$\partial_t\langle\hat{\sigma}_z\rangle = -\Gamma(1 + \langle\hat{\sigma}_z\rangle) - \Omega(t)(\langle\hat{\sigma}_+\rangle + \langle\hat{\sigma}_-\rangle) \tag{4}$$

where $\hat{\sigma}_z$ is the third Pauli spin operator. We numerically solve eqs 3 and 4 with a known arbitrary input waveform $\Omega(t)$ and the parameters in Table 1. All theory curves shown in the whole paper have no free fitting parameters. Since the qubit is initially in the ground state, we have $\langle\hat{\sigma}_\pm(0)\rangle = 0$ and $\langle\hat{\sigma}_z(0)\rangle = -1$. After the pulse stops at t_0, the emission decays

Table 1. Extracted and Derived Qubit Parameters for Samples 1 and 2[a]

sample	distance [mm]	$\omega_{10}/2\pi$ [GHz]	$\Gamma/2\pi$ [MHz]	$\Gamma_{\phi,n}/2\pi$ [MHz]	$\gamma/2\pi$ [MHz]	T_2 [ns]	η [%]	S [%]
1	12	4.8514	1.686 ± 0.007	0.113 ± 0.009	0.956 ± 0.005	166 ± 1	77.7 ± 1.6	88.2 ± 0.8
2	0	4.8187	2.046 ± 0.003	0.031 ± 0.004	1.054 ± 0.003	151 ± 0.4	94.2 ± 0.7	97.1 ± 0.4

[a]Sample 2 has a better loading efficiency (η) and a higher symmetry (S) than sample 1 due to the better ratio of $\Gamma/2\gamma$.

https://doi.org/10.1021/acs.nanolett.2c02578
Nano Lett. 2022, 22, 8137−8142

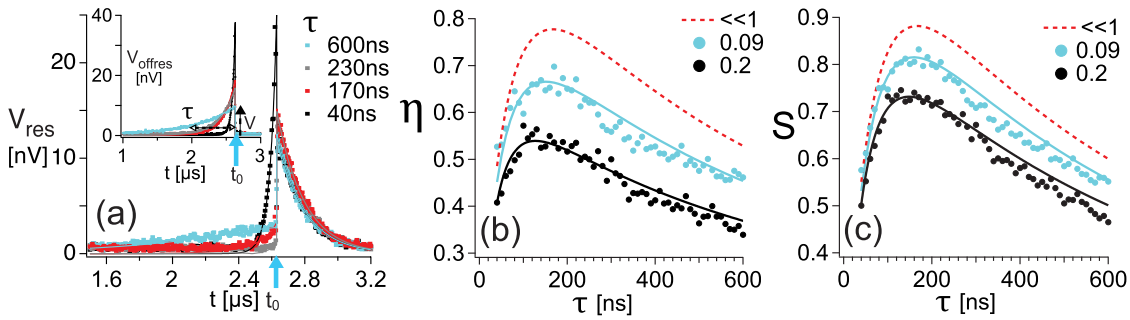

Figure 2. Loading a coherent state with exponentially rising waveforms onto a qubit (sample 1). Experimental data are shown as either square or round markers. Theoretical calculations, based on the parameters in Table 1 and the equations in the main text, are shown as curves. (a) Output magnitude for resonant input V_{res}, where the qubit first absorbs the input field and then emits a field when the pulse stops at $t_0 = 2.63$ μs ($t_0^{res} = 2.64$ μs and $t_0^{offres} = 2.62$ μs; see Section S3 in the Supporting Information). Inset: output magnitude for the off-resonant input pulse (V_{offres}) with four different rise times (40, 170, 230, and 600 ns) with constant $N = 0.09$. A magnification of (a) and the inset are provided in Figure S4 in the Supporting Information. (b) Loading efficiency (η) and (c) symmetry factor (S) as a function of τ for different input photon numbers (N) of 0.09 and 0.2. The maximum loading efficiency (symmetry) occurs around $\tau = T_2$, consistent with the input pulse being the time-reversed version of the output. For higher input power, power broadening of the qubit line width causes the maximum loading efficiency (symmetry) to occur at an earlier time. The red dashed curve shows the analytical result from eq 8 for η and S as a function of τ assuming a weak drive, $N \ll 1$. In Section S3 in the Supporting Information, we show step by step how the raw data in (a) was converted to the values in (b, c).

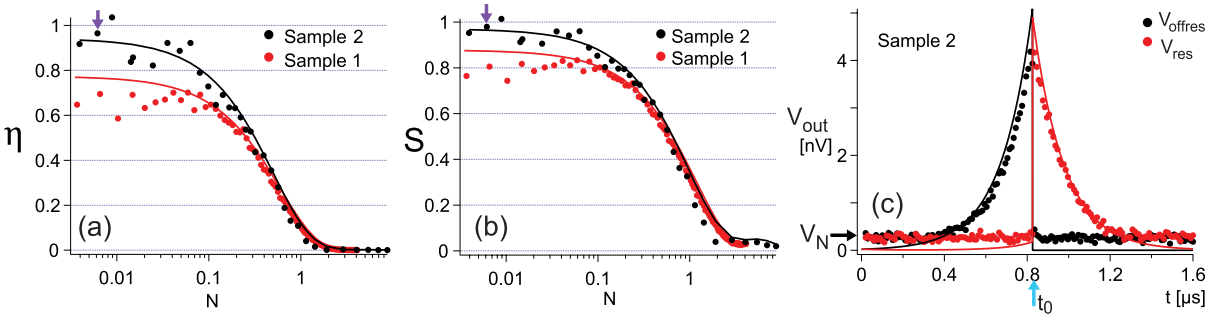

Figure 3. Loading a coherent state with exponentially rising waveforms onto a qubit at fixed $\tau \simeq T_2$. (a) Loading efficiency, η, and (b) symmetry factor, S, as a function of N for samples 1 and 2. As expected, at $N > 1$, incoherent emission becomes dominant,[10] leading to $\eta \to 0$ and $S \to 0$. Note that the revival for S at large N values is due to Rabi oscillations. For $N \ll 1$ and $\tau \simeq T_2$, according to eq 8, $S = \sqrt{\eta}$; this expression also holds when $\tau = 1/\gamma$ only. Therefore, the variations of S and η are related by $\Delta S = \Delta\eta/2$, leading to a larger fluctuation in (a) than (b). In sample 2, for $N \ll 1$, $\eta = 94.2\% \pm 0.7\%$ and $S = 97.1\% \pm 0.4\%$, according to eq 8. (c) Input (black) and emitted (red) voltage at low N values [the point marked by purple arrows in panels (a) and (b)] for sample 2, showing the time-reversal symmetry between the input and output fields. The time resolution for measuring samples 1 and 2 is 5 and 10 ns, respectively. The error in measurement of η and S is mainly from V_N and digitizer resolution.

on the T_2 time scale from $\langle\hat{\sigma}_-(t_0)\rangle$, since $\alpha_{out}(t) = \sqrt{\Gamma}\langle\hat{\sigma}_-(t)\rangle$.

Figure 2a shows the qubit response to off-resonant input (V_{offres}) and on-resonant input (V_{res}), respectively. The 2D plots from which the linecuts in Figure 2a are taken are shown in Figure S3 in the Supporting Information. In the inset of Figure 2a, where the qubit frequency is detuned far away through an external magnetic flux, the output field is assumed to be the reflected input field. Figure 2a consists of two regions: pulse on (absorption) and pulse off (emission). While the drive pulse is being applied, the reflected input pulse and the radiation emitted by the atom interfere destructively, such that no output is measured. One can also understand this as a storage process: the photon is converted into a qubit state, which is emitted back as a photon at a later time. The absorption process corresponds to interference between the incoming field $\alpha_{in}(t)$ and the field $\sqrt{\Gamma}\langle\hat{\sigma}_-(t)\rangle$ emitted from the atom. The emission process corresponds to solely atomic output, which is proportional to $\langle\hat{\sigma}_-\rangle$ and therefore decays on the time scale T_2 indicated by eq 3.

We define the loading efficiency[33,34] as $\eta = E_{res}/E_{offres}$ with

$$E_{offres} \sim \int_{t_i}^{t_0} [|V_{offres}(t)| - |V_N|]^2 \, dt \tag{5}$$

$$E_{res} \sim \int_{t_0}^{t_f} [|V_{res}(t)| - |V_N|]^2 \, dt \tag{6}$$

where V_N is the system voltage noise, E_{res} (E_{offres}) is the energy of the emitted (input) coherent state after (before) t_0, t_i is the time when the input field is turned on, and t_f is the time when we stop collecting the emitted field. The times t_i and t_f are chosen to be when the signal is equal to the noise level, and $t_0 = 2.63$ and 0.825 μs for samples 1 and 2, respectively. We also define the symmetry factor (S) as the correlation between V_{offres} and the time-reversed V_{res}, normalized by the autocorrelation of V_{offres}:

$$S = \frac{\int_{t_i}^{t_0} [|V_{offres}(t)| - |V_N|][|V_{res}(2t_0 - t)| - |V_N|] \, dt}{\int_{t_i}^{t_0} [|V_{offres}(t)| - |V_N|]^2 \, dt} \tag{7}$$

The symmetry factor indicates the degree of symmetry between V_{offres} and V_{res}. Figure 2b,c shows η and S as a function of τ for two different N values for sample 1. The

https://doi.org/10.1021/acs.nanolett.2c02578
Nano Lett. 2022, 22, 8137−8142

maximum loading efficiencies and symmetry factors occur around $\tau = T_2$, consistent with time-reversal symmetry.

Assuming a weak drive $\Omega \ll \gamma$, i.e, $N \ll 1$, the loading efficiency and symmetry factor can be calculated analytically:

$$\eta \simeq \frac{\Gamma^2}{\gamma\tau(\gamma + 1/\tau)^2} \quad S \simeq \frac{2\Gamma}{\tau(\gamma + 1/\tau)^2} \tag{8}$$

These analytical results are plotted as red dashed curves in Figure 2b,c. In Figure 3a,b, for a constant $\tau \simeq T_2$, we show η and S as a function of N for samples 1 and 2. As expected, at large $N \gtrsim 1$, both η and S approach zero. Also, both η and S reach their maxima at small $N < 0.01$, limited by the qubit coherence. With increasing $N < 1$, the high-order photon Fock states become more important, whereas the population for the single-photon Fock state is decreased, leading to a dramatic reduction of η and S, as shown in Figure 3a,b. The details for obtaining Figure 3a,b are shown in Section S3 in the Supporting Information. In Figure 3c, we show the input and emitted signals for points with high η and S values (weak drive $N \approx 0.005$) from sample 2. We observe the time-reversal symmetry between the input and output field.

We demonstrated the efficient loading of a weak coherent state onto a qubit in a 1D semi-open waveguide using a time-reversed waveform. We obtained a loading efficiency of 94.2% ± 0.7% using weak exponentially rising coherent input pulses with characteristic times equal to the qubit decoherence time. The high loading efficiency is due to the time-reversal symmetry between the incoming and emitted waves with symmetry up to 97.1% ± 0.4%, where the loading efficiency can be improved further [see Section S5 in the Supporting Information]. Furthermore, we calculated that our setup with a qubit in front of a mirror also can be loaded with a single Fock-state photon with a deterministic efficiency of 98.5% and symmetry of 99.3% using the parameters measured for sample 2 [see Sections S6−S9 in the Supporting Information].

In conclusion, our results may enable promising applications by realizing deterministic quantum networks based on waveguide quantum electrodynamics. A next step in this direction would be to make the coupling between the qubit and the waveguide tunable to prevent the photon being emitted immediately after it has been absorbed. By placing our qubit in sample 2 in front of a mirror with a certain distance similar to our sample 1, it is possible to suppress the qubit decay by a factor of 50 by tuning the qubit frequency,[13] leading to a storage time of up to $1/(\Gamma/50) \approx 4$ μs. Moreover, the switching time between the node and anti-node can be within nanoseconds.[44] Therefore, such a long storage time with a short flux-switching time enables the possibility of operating the qubit further with an additional separate control line after absorbing single photons, since typical single-qubit gate times are on the order of a few nanoseconds.[45] Finally, the demonstrated method here can in principle also be used for other quantum systems, such as spins[46] and atoms[47] along waveguides.

■ ASSOCIATED CONTENT

Supporting Information

The Supporting Information is available free of charge at https://pubs.acs.org/doi/10.1021/acs.nanolett.2c02578.

Experimental setup and device, steady-state reflection coefficient for extracting parameters of the qubits, full data for loading coherent photons with exponentially rising waveforms onto a qubit, loading a weak coherent state onto a qubit with other waveforms, discussion of optimal loading efficiency and optimal symmetry factor, general formalism for a single-photon pulse (Fock state), output field and loading efficiency, and loading a single-photon Fock state using an exponentially rising waveform and time-reversal symmetry for Fock-state input (PDF)

■ AUTHOR INFORMATION

Corresponding Authors

Io-Chun Hoi − *Department of Physics, City University of Hong Kong, Kowloon, Hong Kong SAR 999077, China; Department of Physics, National Tsing Hua University, Hsinchu 30013, Taiwan;* orcid.org/0000-0002-4636-7110; Email: iochoi@cityu.edu.hk

Yong Lu − *Department of Microtechnology and Nanoscience (MC2), Chalmers University of Technology, SE-412 96 Gothenburg, Sweden; 3rd Institute of Physics, IQST, and Research Centre SCoPE, University of Stuttgart, Stuttgart 70049, Germany*; Email: kdluyong@outlook.com

Authors

Wei-Ju Lin − *Department of Physics, National Tsing Hua University, Hsinchu 30013, Taiwan;* orcid.org/0000-0002-5888-7009

Ping Yi Wen − *Department of Physics, National Chung Cheng University, Chiayi 621301, Taiwan*

Yu-Ting Cheng − *Department of Physics, National Tsing Hua University, Hsinchu 30013, Taiwan;* orcid.org/0000-0001-5996-5585

Ching-Ping Lee − *Department of Physics, National Tsing Hua University, Hsinchu 30013, Taiwan;* orcid.org/0000-0002-1213-5901

Kuan Ting Lin − *CQSE, Department of Physics, National Taiwan University, Taipei 10617, Taiwan*

Kuan Hsun Chiang − *Department of Physics, National Central University, Jhongli 32001, Taiwan*

Ming Che Hsieh − *Department of Physics, National Tsing Hua University, Hsinchu 30013, Taiwan*

Ching-Yeh Chen − *Department of Physics, National Tsing Hua University, Hsinchu 30013, Taiwan*

Chin-Hsun Chien − *Department of Physics, National Tsing Hua University, Hsinchu 30013, Taiwan*

Jia Jhan Lin − *Department of Physics, National Tsing Hua University, Hsinchu 30013, Taiwan*

Jeng-Chung Chen − *Department of Physics, National Tsing Hua University, Hsinchu 30013, Taiwan; Center for Quantum Technology, National Tsing Hua University, Hsinchu 30013, Taiwan*

Yen Hsiang Lin − *Department of Physics, National Tsing Hua University, Hsinchu 30013, Taiwan; Center for Quantum Technology, National Tsing Hua University, Hsinchu 30013, Taiwan*

Chih-Sung Chuu − *Department of Physics, National Tsing Hua University, Hsinchu 30013, Taiwan; Center for Quantum Technology, National Tsing Hua University, Hsinchu 30013, Taiwan*

Franco Nori − *Theoretical Quantum Physics Laboratory, RIKEN Cluster for Pioneering Research, Wako-shi, Saitama 351-0198, Japan; Physics Department, The University of Michigan, Ann Arbor, Michigan 48109-1040, United States;* orcid.org/0000-0003-3682-7432

https://doi.org/10.1021/acs.nanolett.2c02578
Nano Lett. 2022, 22, 8137−8142

Anton Frisk Kockum − *Department of Microtechnology and Nanoscience (MC2), Chalmers University of Technology, SE-412 96 Gothenburg, Sweden;* orcid.org/0000-0002-2534-3021

Guin Dar Lin − *CQSE, Department of Physics, National Taiwan University, Taipei 10617, Taiwan; Physics Division, National Center for Theoretical Sciences, Taipei 10617, Taiwan; Trapped-Ion Quantum Computing Laboratory, Hon Hai Research Institute, Taipei 11492, Taiwan*

Per Delsing − *Department of Microtechnology and Nanoscience (MC2), Chalmers University of Technology, SE-412 96 Gothenburg, Sweden*

Complete contact information is available at: https://pubs.acs.org/10.1021/acs.nanolett.2c02578

Author Contributions

○W.-J.L., Y.L., and P.Y.W. contributed equally to this work.

Notes

The authors declare no competing financial interest.

■ ACKNOWLEDGMENTS

I.-C.H. and J.-C.C. thank I.A. Yu for fruitful discussions. We also acknowledge IARPA and Lincoln Laboratories for providing the TWPA used in this experiment. This work was financially supported by the Center for Quantum Technology from the Featured Areas Research Center Program within the framework of the Higher Education Sprout Project by the Ministry of Education (MOE) in Taiwan. I.-C.H. acknowledges financial support from the MOST of Taiwan under project 109-2636-M-007-007 and from City University of Hong Kong through the start-up project 9610569. G.D.L. acknowledges support from MOST, Taiwan, under Grant No. 109-2112-M-002-022, and NTU under Grant No. NTU-CC-110L890106. P.Y.W. acknowledges support from NSTC, Taiwan, under Grant No. 110-2112-M-194-006-MY3. A.F.K., Y.L., and P.D. acknowledge support from the Knut and Alice Wallenberg Foundation through the Wallenberg Centre for Quantum Technology (WACQT) and from the Swedish Research Council (Grant Numbers 2019-03696 and 2015-00152, respectively). F.N. is supported in part by Nippon Telegraph and Telephone Corporation (NTT) Research, the Japan Science and Technology Agency (JST) [via the Quantum Leap Flagship Program (Q-LEAP)], the Moonshot R&D Grant Number JPMJMS2061, the Japan Society for the Promotion of Science (JSPS) [via the Grants-in-Aid for Scientific Research (KAKENHI) Grant No. JP20H00134], the Army Research Office (ARO) (Grant No. W911NF-18-1-0358), the Asian Office of Aerospace Research and Development (AOARD) (via Grant No. FA2386-20-1-4069), and the Foundational Questions Institute Fund (FQXi) via Grant No. FQXi-IAF19-06.

■ REFERENCES

(1) Kimble, H. J. The quantum internet. *Nature* **2008**, *453*, 1023.

(2) Wehner, S.; Elkouss, D.; Hanson, R. Quantum internet: A vision for the road ahead. *Science* **2018**, *362*, No. eaam9288.

(3) Tey, M. K.; Chen, Z.; Aljunid, S. A.; Chng, B.; Huber, F.; Maslennikov, G.; Kurtsiefer, C. Strong interaction between light and a single trapped atom without the need for a cavity. *Nat. Phys.* **2008**, *4*, 924.

(4) Zhang, S.; Liu, C.; Zhou, S.; Chuu, C.-S.; Loy, M. M. T.; Du, S. Coherent control of single-photon absorption and reemission in a two-level atomic ensemble. *Phys. Rev. Lett.* **2012**, *109*, 263601.

(5) Astafiev, O.; Zagoskin, A. M.; Abdumalikov, A. A.; Pashkin, Y. A.; Yamamoto, T.; Inomata, K.; Nakamura, Y.; Tsai, J. S. Resonance Fluorescence of a Single Artificial Atom. *Science* **2010**, *327*, 840.

(6) Hoi, I.-C.; Wilson, C. M.; Johansson, G.; Palomaki, T.; Peropadre, B.; Delsing, P. Demonstration of a Single-Photon Router in the Microwave Regime. *Phys. Rev. Lett.* **2011**, *107*, 073601.

(7) Gu, X.; Kockum, A. F.; Miranowicz, A.; Liu, Y.-X.; Nori, F. Microwave photonics with superconducting quantum circuits. *Phys. Rep.* **2017**, *718−719*, 1−102.

(8) Frisk Kockum, A.; Nori, F.Quantum Bits with Josephson Junctions. In *Fundamentals and Frontiers of the Josephson Effect*; Springer Series in Materials Science; Springer: Cham, 2019; Vol *286*.

(9) Roy, D.; Wilson, C. M.; Firstenberg, O. Colloquium: Strongly interacting photons in one-dimensional continuum. *Rev. Mod. Phys.* **2017**, *89*, 021001.

(10) Hoi, I.-C.; Palomaki, T.; Lindkvist, J.; Johansson, G.; Delsing, P.; Wilson, C. M. Generation of Nonclassical Microwave States Using an Artificial Atom in 1D Open Space. *Phys. Rev. Lett.* **2012**, *108*, 263601.

(11) van Loo, A. F.; Fedorov, A.; Lalumiere, K.; Sanders, B. C.; Blais, A.; Wallraff, A. Photon-Mediated Interactions Between Distant Artificial Atoms. *Science* **2013**, *342*, 1494.

(12) Hoi, I.-C.; Kockum, A. F.; Palomaki, T.; Stace, T. M.; Fan, B.; Tornberg, L.; Sathyamoorthy, S. R.; Johansson, G.; Delsing, P.; Wilson, C. M. Giant Cross-Kerr Effect for Propagating Microwaves Induced by an Artificial Atom. *Phys. Rev. Lett.* **2013**, *111*, 053601.

(13) Hoi, I.-C.; Kockum, A. F.; Tornberg, L.; Pourkabirian, A.; Johansson, G.; Delsing, P.; Wilson, C. M. Probing the quantum vacuum with an artificial atom in front of a mirror. *Nat. Phys.* **2015**, *11*, 1045.

(14) Forn-Díaz, P.; García-Ripoll, J. J.; Peropadre, B.; Orgiazzi, J.-L.; Yurtalan, M. A.; Belyansky, R.; Wilson, C. M.; Lupascu, A. Ultrastrong coupling of a single artificial atom to an electromagnetic continuum in the nonperturbative regime. *Nat. Phys.* **2017**, *13* (39), 39.

(15) Frisk Kockum, A.; Miranowicz, A.; De Liberato, S.; Savasta, S.; Nori, F. Ultrastrong coupling between light and matter. *Nature Reviews Physics* **2019**, *1*, 19.

(16) Wen, P. Y.; Kockum, A. F.; Ian, H.; Chen, J. C.; Nori, F.; Hoi, I.-C. Reflective Amplification without Population Inversion from a Strongly Driven Superconducting Qubit. *Phys. Rev. Lett.* **2018**, *120*, 063603.

(17) Wen, P. Y.; Lin, K.-T.; Kockum, A. F.; Suri, B.; Ian, H.; Chen, J. C.; Mao, S. Y.; Chiu, C. C.; Delsing, P.; Nori, F.; Lin, G.-D.; Hoi, I.-C. Large Collective Lamb Shift of Two Distant Superconducting Artificial Atoms. *Phys. Rev. Lett.* **2019**, *123*, 233602.

(18) Mirhosseini, M.; Kim, E.; Zhang, X.; Sipahigil, A.; Dieterle, P. B.; Keller, A. J.; Asenjo-Garcia, A.; Chang, D. E.; Painter, O. Cavity quantum electrodynamics with atom-like mirrors. *Nature* **2019**, *569*, 692.

(19) Wen, P. Y.; Ivakhnenko, O. V.; Nakonechnyi, M. A.; Suri, B.; Lin, J.-J.; Lin, W.-J.; Chen, J. C.; Shevchenko, S. N.; Nori, F.; Hoi, I.-C. Landau-Zener-Stückelberg-Majorana interferometry of a superconducting qubit in front of a mirror. *Phys. Rev. B* **2020**, *102*, 075448.

(20) Shevchenko, S. N.; Ashhab, S.; Nori, F. Landau−Zener−Stückelberg interferometry. *Phys. Rep.* **2010**, *492*, 1.

(21) Kannan, B.; Ruckriegel, M. J.; Campbell, D. L.; Kockum, A. F.; Braumüller, J.; Kim, D. K.; Kjaergaard, M.; Krantz, P.; Melville, A.; Niedzielski, B. M.; Vepsäläinen, A.; Winik, R.; Yoder, J. L.; Nori, F.; Orlando, T. P.; Gustavsson, S.; Oliver, W. D. Waveguide quantum electrodynamics with superconducting artificial giant atoms. *Nature* **2020**, *583*, 775.

(22) Kockum, A. F.; Johansson, G.; Nori, F. Decoherence-free interaction between giant atoms in waveguide quantum electrodynamics. *Phys. Rev. Lett.* **2018**, *120*, 140404.

(23) Vadiraj, A. M.; Ask, A.; McConkey, T. G.; Nsanzineza, I.; Chang, C. W. S.; Kockum, A. F.; Wilson, C. M. Engineering the level structure of a giant artificial atom in waveguide quantum electrodynamics. *Phys. Rev. A* **2021**, *103*, 023710.

(24) Abdumalikov, A. A.; Astafiev, O. V.; Pashkin, Y. A.; Nakamura, Y.; Tsai, J. S. Dynamics of coherent and incoherent emission from an artificial atom in a 1D space. *Phys. Rev. Lett.* **2011**, *107*, 043604.
(25) Leong, V.; Seidler, M. A.; Steiner, M.; Cere, A.; Kurtsiefer, C. Time-resolved scattering of a single photon by a single atom. *Nat. Commun.* **2016**, *7*, 13716.
(26) Aljunid, S. A.; Maslennikov, G.; Wang, Y.; Dao, H. L.; Scarani, V.; Kurtsiefer, C. Excitation of a Single Atom with Exponentially Rising Light Pulses. *Phys. Rev. Lett.* **2013**, *111*, 103001.
(27) Wang, Y.; Minar, J.; Sheridan, L.; Scarani, V. Efficient excitation of a two-level atom by a single photon in a propagating mode. *Phys. Rev. A* **2011**, *83*, 063842.
(28) Peng, Z. H.; De Graaf, S. E.; Tsai, J. S.; Astafiev, O. V. Tuneable on-demand single-photon source in the microwave range. *Nat. Commun.* **2016**, *7*, 12588.
(29) Zhou, Y.; Peng, Z.; Horiuchi, Y.; Astafiev, O.V.; Tsai, J.S. Tunable microwave single-photon source based on transmon qubit with high efficiency. *Physical Review Applied* **2020**, *13*, 2.
(30) Pechal, M.; Besse, J. C.; Mondal, M.; Oppliger, M.; Gasparinetti, S.; Wallraff, A. Superconducting switch for fast on-chip routing of quantum microwave fields. *Physical Review Applied* **2016**, *6*, 024009.
(31) Lu, Y.; Bengtsson, A.; Burnett, J. J.; Suri, B.; Sathyamoorthy, S. R.; Nilsson, H. R.; Scigliuzzo, M.; Bylander, J.; Johansson, G.; Delsing, P. Quantum efficiency, purity and stability of a tunable, narrowband microwave single-photon source. *npj Quantum Information* **2021**, *7*, 12.
(32) Forn-Díaz, P.; Warren, C. W.; Chang, C. W.S.; Vadiraj, A. M.; Wilson, C. M. On-demand microwave generator of shaped single photons. *Physical Review Applied* **2017**, *8*, 11.
(33) Liu, C.; Sun, Y.; Zhao, L.; Zhang, S.; Loy, M. M. T.; Du, S. Efficiently Loading a Single Photon into a Single-Sided Fabry-Perot Cavity. *Phys. Rev. Lett.* **2014**, *113*, 133601.
(34) Wenner, J.; Yin, Y.; Chen, Y.; Barends, R.; Chiaro, B.; Jeffrey, E.; Kelly, J.; Megrant, A.; Mutus, J. Y.; Neill, C.; O'Malley, P. J. J.; Roushan, P.; Sank, D.; Vainsencher, A.; White, T. C.; Korotkov, A. N.; Cleland, A. N.; Martinis, J. M. Catching time-reversed microwave coherent state photons with 99.4% absorption efficiency. *Phys. Rev. Lett.* **2014**, *112*, 210501.
(35) Pierre, M.; Sathyamoorthy, S. R.; Svensson, I.-M.; Johansson, G.; Delsing, P. Resonant and off-resonant microwave signal manipulation in coupled superconducting resonators. *Phys. Rev. B* **2019**, *99*, 094518.
(36) Kurpiers, P.; Magnard, P.; Walter, T.; Royer, B.; Pechal, M.; Heinsoo, J.; Salathé, Y.; Akin, A.; Storz, S.; Besse, J.-C.; Gasparinetti, S.; Blais, A.; Wallraff, A. Deterministic quantum state transfer and remote entanglement using microwave photons. *Nature* **2018**, *558*, 264.
(37) Zhong, Y.; Chang, H.-S.; Bienfait, A.; Dumur, E.; Chou, M.-H.; Conner, C. R.; Grebel, J.; Povey, R. G.; Yan, H.; Schuster, D. I.; Cleland, A. N. Deterministic multi-qubit entanglement in a quantum network. *Nature* **2021**, *590*, 571.
(38) Koch, J.; Yu, T. M.; Gambetta, J.; Houck, A. A.; Schuster, D. I.; Majer, J.; Blais, A.; Devoret, M. H.; Girvin, S. M.; Schoelkopf, R. J. Charge-insensitive qubit design derived from the Cooper pair box. *Phys. Rev. A* **2007**, *76*, 042319.
(39) Lu, Y.; Strandberg, I.; Quijandria, F.; Johansson, G.; Gasparinetti, S.; Delsing, P. Propagating Wigner-negative states generated from the steady-state emission of a superconducting qubit. *Phys. Rev. Lett.* **2021**, *126*, 253602.
(40) Probst, S.; Song, F. B.; Bushev, P. A.; Ustinov, A. V.; Weides, M. Efficient and robust analysis of complex scattering data under noise in microwave resonators. *Rev. Sci. Instrum.* **2015**, *86*, 024706.
(41) Lu, Y.; Bengtsson, A.; Burnett, J. J.; Wiegand, E.; Suri, B.; Krantz, P.; Roudsari, A. F.; Kockum, A. F.; Gasparinetti, S.; Johansson, G.; Delsing, P. Characterizing decoherence rates of a superconducting qubit by direct microwave scattering. *npj Quantum Information* **2021**, *7*, 35.
(42) The anharmonicity of our transmon is a few hundred times larger than the line width of the loading pulse. Moreover, since we use a very weak coherent state, the atom is mostly in its ground state. Even when the photon number (N) equals 1, the population in the second excited state $|2\rangle$is only about 0.01% of the population in the first excited state $|1\rangle$due to the anharmonicity. This is the numerical result from solving the multilevel optical Bloch equations.[48] Therefore, we can neglect the effect of higher levels.
(43) Lalumière, K.; Sanders, B. C.; van Loo, A. F.; Fedorov, A.; Wallraff, A.; Blais, A. Input-output theory for waveguide QED with an ensemble of inhomogeneous atoms. *Phys. Rev. A* **2013**, *88*, 043806.
(44) Sandberg, M.; Wilson, C. M.; Persson, F.; Bauch, T.; Johansson, G.; Shumeiko, V.; Duty, T.; Delsing, P. Tuning the field in a microwave resonator faster than the photon lifetime. *Appl. Phys. Lett.* **2008**, *92*, 203501.
(45) Werninghaus, M.; Egger, D. J.; Roy, F.; Machnes, S.; Wilhelm, F. K.; Filipp, S. Leakage reduction in fast superconducting qubit gates via optimal control. *npj Quantum Information* **2021**, *7* (1), 14.
(46) Babin, C.; Stohr, R.; Morioka, N.; Linkewitz, T.; Steidl, T.; Wornle, R.; Liu, D.; Hesselmeier, E.; Vorobyov, V.; Denisenko, A.; Hentschel, M.; Gobert, C.; Berwian, P.; Astakhov, G. V.; Knolle, W.; Majety, S.; Saha, P.; Radulaski, M.; Son, N. T.; Ul-Hassan, J.; Kaiser, F.; Wrachtrup, J. Fabrication and nanophotonic waveguide integration of silicon carbide colour centres with preserved spin-optical coherence. *Nature materials* **2022**, *21*, 67−73.
(47) Ovchinnikov, Y. B. A perspective on integrated atomo-photonic waveguide circuits. *Appl. Phys. Lett.* **2022**, *120* (1), 010502.
(48) Lin, K.-T.; Hsu, T.; Lee, C.-Y.; Hoi, I.-C.; Lin, G.-D. Scalable collective lamb shift of a 1d superconducting qubit array in front of a mirror. *Sci. Rep.* **2019**, *9*, 19175.

https://doi.org/10.1021/acs.nanolett.2c02578
Nano Lett. 2022, 22, 8137−8142